Available online at www.sciencedirect.com

ScienceDirect

Solar Energy 00 (2018) 1–17

Solar Energy

A Novel Adaptive Command-Filtered Backstepping Sliding Mode Control for PV Grid-Connected System with Energy Storage

Dezhi Xu[a,*], Gang Wang[a], Wenxu Yan[a], Xinggang Yan[b]

[a]*School of Internet of Things Engineering (Institute of Electrical Engineering and Intelligent Equipment), Jiangnan University, Wuxi, 214122, China*

[b]*School of Engineering and Digital Arts, University of Kent, Canterbury, CT2 7NT, U.K.*

Abstract

To solve the problems of power fluctuation in the photovoltaic (PV) grid-connected system and the nonlinearity in the model of inverters, a projection-based adaptive backstepping sliding mode controller with command-filter is designed in the system, in order to adjust the DC-link voltage and the AC-side current in the PV grid-connected system. Firstly, the mathematic model of the inverter in PV system is established, then backstepping control method is applied to control it, and the command filter is added to the controller to eliminate the differential expansion of the backstepping controller. Furthermore, the adaptive law based on Lyapunov stability theory is designed to estimate the uncertain parameters in the grid-connected inverter. A projection algorithm is introduced in the adaptive controller due to the demand of guaranteeing the bounded estimated value. Additionally, a sliding mode controller is increased to improve its robustness in this system.With the consideration of the influence of irradiation and temperature changes, a battery-energy-storage-system is applied to the DC-side to suppress the fluctuation of output power of the PV system. Finally, the simulation results demonstrate that the presented strategy can control the grid connected inverter precisely.

Keywords: Photovoltaic system, battery energy storage, projection adaptive, command-filtered backstepping, sliding mode.

1. Introduction

Nowadays, because of the rapid growth of the grid-connected photovoltaic (PV) system, the controller of the system is confronted with the tremendous challenges of maintaining grid stability and reliability [1]. In Fig. 1, two key factors of the energy storage PV grid-connected system should be realized [2]. The first factor is the effects of weather conditions which include irradiation, temperature and some other meteorological conditions. Another factor is the impact of the inverter, the PV controller and the load in the system [3-4]. Obviously, the weather conditions are uncontrollable, so a battery-energy-storage-system is considered in the DC side of the PV system to compensate the fluctuation of output power of PV system when the irradiation and temperature are changing [5-6]. At same time, it is necessary to design and control the inverter effectively to ensure the output power quality of the PV system. The grid converts the maximum power of a PV power generation system into the high power quality, which is the primary goal of a PV grid-connected power generation system, i.e., despite of the changes in atmospheric conditions, the power factor of PV grid-connected system is closed to unity. This requires that the inverter switch would be designed to inject no harmonic current into the grid [7-8].

*Corresponding author

Email address: xudezhi@jiangnan.edu.cn, lutxdz@126.com (Dezhi Xu)

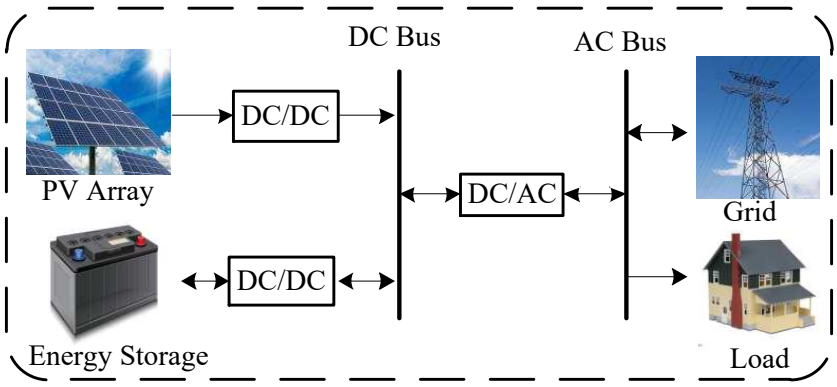

Figure 1: Topology of PV power system with energy storage.

A lot of efforts have been devoted to PV micro-grid in the past. In reference [9], a fractional order sliding mode controller was applied to an islanded distributed energy resource system, and the output voltage tracking control was realized. However, in the simulation, the authors used the DC source instead of the distributed energy.When the PV array was connected to the DC side of the system, the control effect of the designed controller was unknown. The work in [10] proposed a voltage and frequency control strategy for the distributed energy resource system, different types of loads were used to be simulated the control effect, and the parallel operation of multiple distributed-resource units was simulated. However, there was no use of the distributed energy resource in the author's simulation, and the energy storage unit was not considered in the system. Also in the work of [11], the maximum power point tracking (MPPT) was realized through the use of sliding mode control. Then the Lyapunov function-based control method was utilized in VSC, the simulation showed that the controller had better control effect. However, the control algorithm presented in this work possessed some limitations, and the control effect also had space for improvement, in addition, the energy storage unit was also not considered in the system.

At present, the linear control theory has been widely investigated to power converters [12-14]. Due to the dynamic of the power, converters are nonlinear, and some parameters cannot be measured accurately. Hence, a large number of nonlinear control methods are introduced to solve problems of the nonlinearity and uncertainty of power converters [15-21]. As a kind approach of nonlinear control, the backstepping which is widely used in grid-connected system is considered to deal with the nonlinearity and uncertainty [20-22]. In [23], the backstepping controller is designed in the PV power supply system of telecommunication equipment. By controlling the DC-DC buck-boost circuit, the DC side voltage is stable, and it ensures that the total harmonic misalignment rate of the AC side is within the s-cope. Consequently, the effectiveness of the backstepping controller is verified by simulation. In order to estimate the unknown parameters in the system, adaptive backstepping approach has been proposed, and this strategy which can achieve satisfactory control performance is proved to be effective[24]. In [25], an adaptive backstepping controller is designed for permanent magnet linear synchronous motor, and the tracking of the motor position is realized. Experi-ment shows that the control effect of designed adaptive backstepping controller is better than proportion-integral (PI) controller. However, on account of some main drawbacks of the backstepping control, such as the derivative of the virtual control and problems of control saturation, which can increase the amount of calculation and affect the control effect of the controller. Some methods have been put forward to solve this shortcoming, such as the dynamic surface control [26] and the command-filter [27-28], in which command-filtered backstepping is more effective than dynamic surface control. The amplitude, speed and bandwidth constraints are introduced into the command filtering process, which are more convenient for modulation and restriction of virtual control signals and actual control signals so as to meet the actual control requirements [29].

In this paper, an improved adaptive command-filtered backstepping controller is designed for inverter of battery-energy-storage-system with PV (BESS-PV) grid-connected system, which is used to stabilize DC side voltage and control output power of PV system. In this proposed controller, an adaptive law based on Lyapunov stability theory is introduced to estimate the uncertain parameters (including DC-link capacitor, output resistance and inductance) of

grid-connected inverter. Considering the demand of guaranteeing for the bounded estimated value, a projection algorithm is proposed in the adaptive law. Additionally, the integral sliding mode control method is added to the control system for improving the robustness of close-loop control systems. In the controller design procedure, the command filter and compensation are used to solve the problems of the differential expansion about virtual control signal and the control input saturation. At same time, the stability of the control system is presented to be asymptotically stable by using the Lyapunov stability theory. In section II, the model of inverter in PV system is established. In section III, the controller is derived and the stability of the system is proved by Lyapunov stability theory. In section IV, the advanced nature of the designed controller is demonstrated in MATLAB/simulink. Finally, some conclusions are given in section V.

2. PV Grid-Connected System Model

2.1. PV Cell and Array Modeling

Fig. 2 shows a circuit diagram of a photovoltaic cell. The diode current I_D can be written as [30-31]

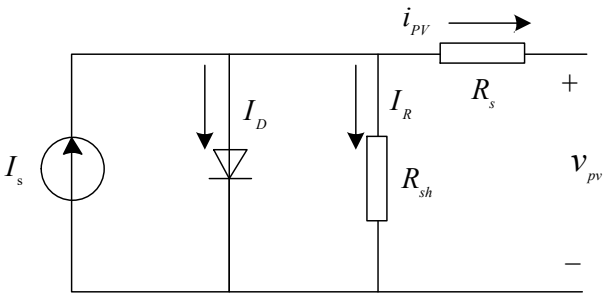

Figure 2: Circuit diagram of a PV cell.

$$I_D = I_0\left(\exp\left(\frac{q\left(v_{pv}+R_s i_{pv}\right)}{AkT}\right)-1\right) \tag{1}$$

where I_s is the photocurrent, R_{sh} is the shunt resistor, R_s is the shunt resistance, q is the electron charge which $q = 1.6\times10^{19}$ C, I_0 is the reverse saturation current, A is the dimensionless junction material factor, k is the Boltzmann constant, and T is operating temperature of solar cell (in Kelvin).

Now, in Fig. 2, the Kirchhoff's law of current is applied, and the output current of i_{pv} produced by the PV battery can be expressed as

$$i_{pv} = I_s - I_0\left(\exp\left(\frac{q\left(v_{pv}+R_s i_{pv}\right)}{AkTN_s}\right)-1\right)-\frac{v_{pv}+R_s i_{pv}}{R_{sh}} \tag{2}$$

The luminous current I_s depends on the solar radiation which can be associated with

$$I_s = \left(I_{sc}+k_i\left(T-T_n\right)\right)\frac{R}{R_n} \tag{3}$$

where I_{sc} is the short-circuit current, R is the solar radiation, k_i is the parameter of PV cell short-circuit current, and T_n is the reference temperature of PV cell. The saturation current changing with the temperature of the cell is I_0 with

$$I_0 = I_{RS}\left(\frac{T}{T_n}\right)^3\exp\left[\frac{qE_g}{Ak}\left(\frac{1}{T_n}-\frac{1}{T}\right)\right] \tag{4}$$

where E_g is the PV cell semiconductor band-gap energy. I_{RS} is the reverse saturation current under the reference temperature and the irradiation.

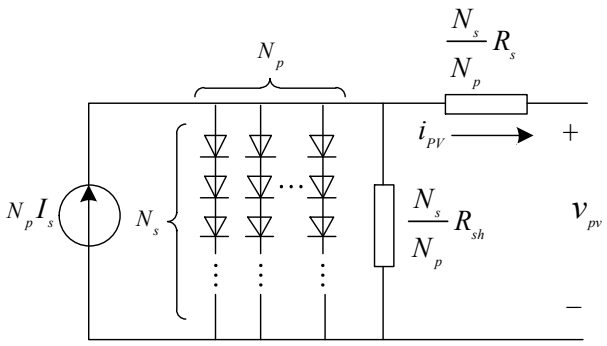

Figure 3: Circuit diagram of a PV array.

Photovoltaic cells are usually connected in series and in parallel to form PV array which can help get the power. Fig. 3 represents the circuit diagram of a PV array, where N_s and N_p are the series and parallel number of PV cells, respectively. In this way, the output current i_{pv} can be written as

$$i_{pv} = N_p I_s - N_p I_D \left(\exp\left(\frac{q\left(v_{pv} + R_s i_{pv}\right)}{AkTN_s} \right) - 1 \right) - N_p \frac{v_{pv} + R_s i_{pv}}{N_s R_{sh}} \tag{5}$$

The manufacturing characteristics of each PV cell are given in Table 1. The power of the entire photovoltaic array is: $5 \cdot 66 \cdot 302.226 \approx 100.7kW$. The power-voltage (P-V) performance characteristic under different weather conditions of a given PV array are shown in Fig. 4.

Table 1: The Basic Parameters of The PV Cell

Parameter	Symbol	Value
Maximum output power	P_p	302.226 (W)
Open circuit voltage	V_{oc}	64.2 (V)
short-circuit current	I_{sc}	5.96 (A)
Voltage at maximum power point	V_{mp}	54.7 (V)
Current at maximum power point	I_{mp}	5.58 (A)
Number of cells in series	N_s	5
Number of cells in parallel	N_p	66

As illustrated in Fig. 4, the maximum power point varies with the weather conditions. The power converter switch is controlled by the MPPT approach to map the maximum output power of the PV array. In the simulation of this study, we use incremental conductance algorithm to realize the control of MPPT. As Fig.4 shows that the output power P, current I and voltage U of PV array have the following relationship

$$P = UI \tag{6}$$

If the irradiance and temperature remain the same, the derivative at the maximum power point of the P-V curve at this irradiance and temperature is 0. So, we need to calculate the derivative of (6)

$$\frac{dP}{dU} = I + U\frac{dI}{dU} = 0 \tag{7}$$

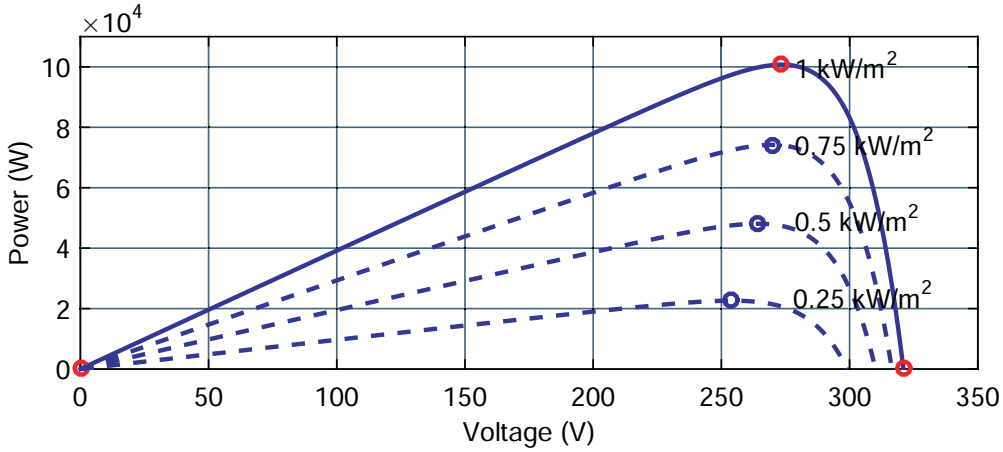

(a) P-V charateristics of array at 25 deg.C.

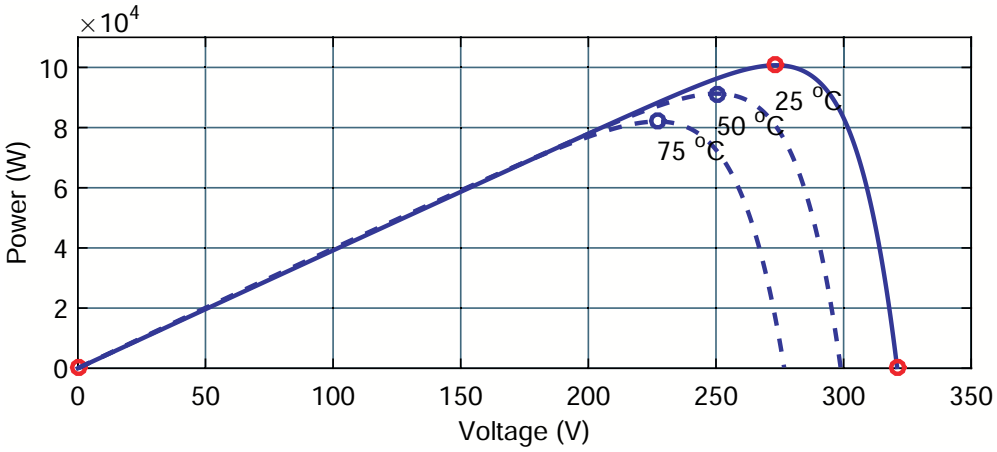

(b) P-V charateristics of array at 1000 W/m^2.

Figure 4: P-V charateristics of a PV array.

then, the relationship can be achieved

$$\frac{dI}{dU} = -\frac{I}{U} \tag{8}$$

when the change rate of output voltage is equal to the negative value of transient conductance of the output, we can make sure that the PV array is works at the maximum power point. We need to sample the voltage and current of PV array. Because the method has high control precision and fast response speed, it is suitable for occasions with relatively rapid changes in atmospheric conditions.

2.2. Energy Management Strategy of BESS

Due to the changeable environment of weather, such as the uncertainty of light radiation and temperature, which lead to the fluctuation of grid-connected power. Therefore, in this paper, we incorporate a rechargeable battery module on the DC side to ensure power stability of PV grid-connected system disturbance when light radiation and temperature are changing.

A simple energy management strategy of PV and BESS module on the DC side is given in Fig. 5. In practical applications, reducing the charge and discharge times of the battery energy storage system must also be considered. In Fig. 5, P_g represents the power requirement of the grid, P_{pv} represents the power which is provided by PV array, P_{bt} is the power of the battery module.

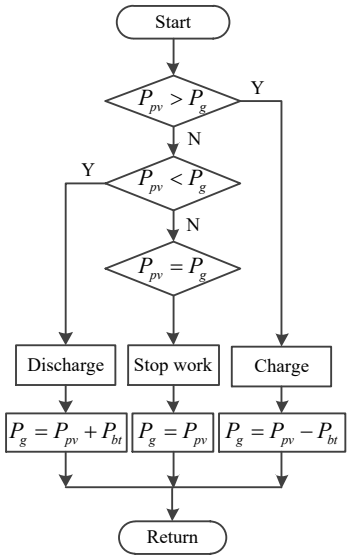

Figure 5: Energy management strategy of BESS.

2.3. Description of PV Grid-Connected System

Fig. 6 shows the diagram of the structure about the grid connected BESS-PV system, which includes PV array, filter capacitor, output R-L filter, inverter, and three-phase grid. Then, the dynamics model of grid-connected dc-to-ac inverter system under d-q frame can be calculated as

$$\begin{aligned} \frac{di_d}{dt} &= -\frac{R}{L}i_d + \omega i_q - \frac{E_d}{L} + \frac{u_{dc}}{L}k_d \\ \frac{di_q}{dt} &= -\frac{R}{L}i_q - \omega i_d - \frac{E_d}{L} + \frac{u_{dc}}{L}k_q \end{aligned} \tag{9}$$

where E_d, E_q and i_d, i_q are the grid voltages and currents under dq-axis, respectively. k_d and k_q are the dq-frame components switching function, respectively.

According to Kirchhoff's voltage and current laws, the relationship in the DC side of inverter is expressed as

$$C\frac{du_{dc}}{dt} = i_0 - i_{dc} \tag{10}$$

therein u_{dc} is the DC-link voltage, i_0 and i_{dc} are the output current of the boost circuit and the input current of the inverter, respectively.

According to the conservation of energy, if the power loss of inverter is neglected, the power balanced relation between the system output and the DC side is provided as

$$u_{dc}i_0 = \frac{3}{2}\left(E_d I_d + E_q I_q\right) \tag{11}$$

However, the average value of E_q is equivalent to zero in a steady state. Then, submitting (11) to (10), the DC-link voltage dynamic is expressed by following

$$\frac{du_{dc}}{dt} = \frac{3E_d I_d}{2Cu_{dc}} - \frac{i_{dc}}{C} \tag{12}$$

Now, the full dynamic model of inverter for PV grid-connected system can be represented as

$$\begin{aligned}\frac{du_{dc}}{dt} &= \frac{3E_d i_d}{2Cu_{dc}} - \frac{i_{dc}}{C}\\ \frac{di_d}{dt} &= -\frac{R}{L}i_d + \omega i_q - \frac{E_d}{L} + \frac{u_d}{L}\\ \frac{di_q}{dt} &= -\frac{R}{L}i_q - \omega i_d - \frac{E_q}{L} + \frac{u_q}{L}\end{aligned} \tag{13}$$

In the above mathematical model, the R, L, and C are the values of resistance, inductance, and capacitance in the system.

In fact, it is very difficult to measure the value of the parameter accurately in the system. Therefore, in the design of the controller, these parameters can be regarded as unknown or uncertain, which can be written as following

$$\eta_1 = \frac{1}{C},\ \eta_2 = \frac{R}{L},\ \eta_3 = \frac{1}{L} \tag{14}$$

Submitting (14) into (13), equation (13) can be rewritten as

$$\begin{aligned}\frac{du_{dc}}{dt} &= \eta_1\left(\frac{3E_d i_d}{2u_{dc}} - i_{dc}\right)\\ \frac{di_d}{dt} &= -\eta_2 i_d + \omega i_q - \eta_3 E_d + \eta_3 u_d\\ \frac{di_q}{dt} &= -\eta_2 i_q - \omega i_d - \eta_3 E_q + \eta_3 u_q\end{aligned} \tag{15}$$

In the section III, we will design the controller based on this model (15) with unknown parameters. Since the sliding mode control has strong robustness [32], we provide an novel projection-based adaptive command-filtered backstepping controller with sliding mode, and which willbe discussed in the following sections.

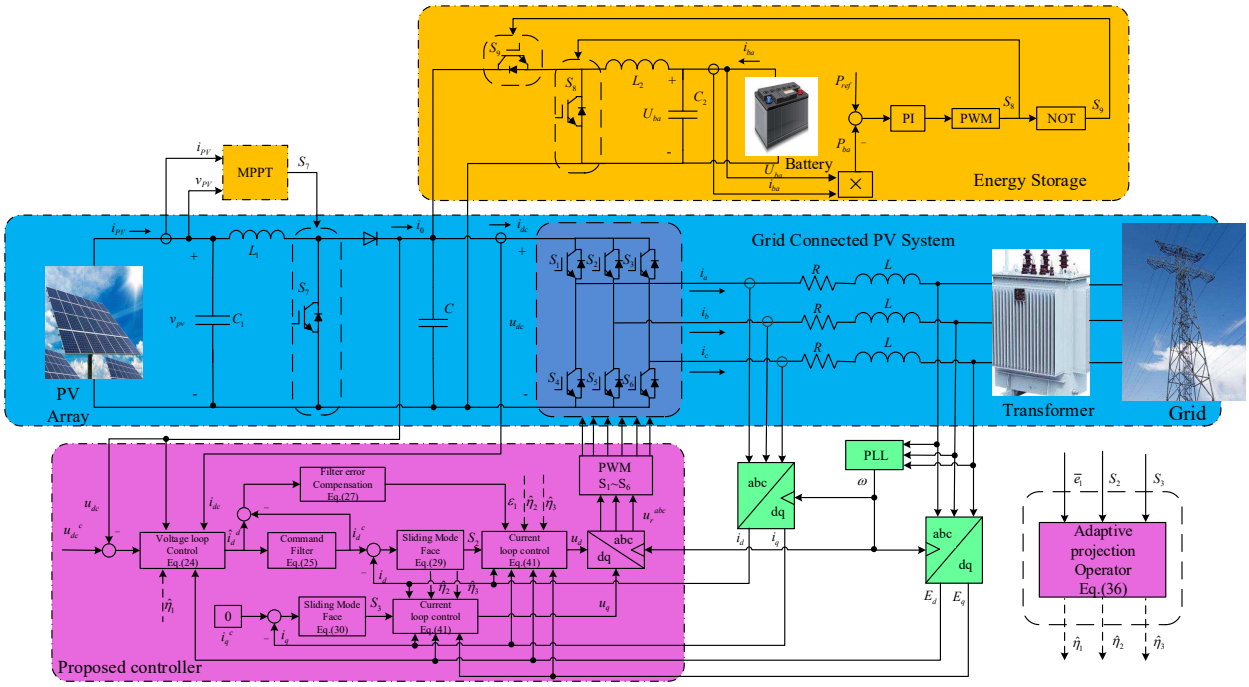

Figure 6: The structure of the proposed controller for BESS-PV grid-connected system.

3. Proposed Controller Design

3.1. Controller Design for Grid-Connected Inverter

In this section, in order to inject the expected reactive and active power into the power grid, the control law u_d and u_q are designed to make the reference value of i_d and i_q. Take the following steps to get the controller.

Firstly, we define the tracking error of the system as

$$e_1 = u_{dc} - u_{dc}^c \tag{16}$$

$$e_2 = i_d - i_d^c \tag{17}$$

$$e_3 = i_q - i_q^c \tag{18}$$

In order to stabilize the DC bus voltage error, the Lyapunov function is selected as

$$V_1 = \frac{1}{2}{e_1}^2 \tag{19}$$

By substituting the value of u_{dc} in (15) into (16), we can write that

$$\dot{e}_1 = \eta_1 \left(\frac{3E_d i_d}{2u_{dc}} - i_{dc} \right) - \dot{u}_{dc}^c \tag{20}$$

Now the derivative of V_1 can be written as

$$\dot{V}_1 = e_1 \dot{e}_1 = e_1 \left(\eta_1 \left(\frac{3E_d i_d}{2u_{dc}} - i_{dc} \right) - \dot{u}_{dc}^c \right) \tag{21}$$

In order to satisfy Lyapunov stability condition, we want to make sure that $\dot{V}_1 \leq 0$, thus we choose the virtual controller i_d^d as

$$i_d^d = \frac{2u_{dc}}{3E_d \eta_1} (\eta_1 i_{dc} + \dot{u}_{dc}^c - k_1 e_1) \tag{22}$$

where $k_1 > 0$ is a designed constant. Then, by inserting the equation (22) into equation (21), $\dot{V}_1$ can be calculated as

$$\dot{V}_1 = -k_1 e_1^2 \tag{23}$$

Because the parameters η_1 is unknown, we replace η_1 with $\hat{\eta}_1$ in equation (22), that is

$$\hat{i}_d^d = \frac{2u_{dc}}{3E_d \hat{\eta}_1} (\hat{\eta}_1 i_{dc} + \dot{u}_{dc}^c - k_1 e_1) \tag{24}$$

where $\tilde{\eta}_1 = \eta_1 - \hat{\eta}_1$ is the parameter estimation error.

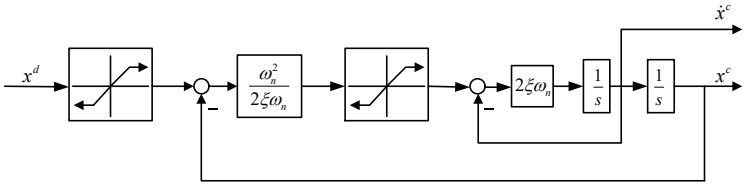

Figure 7: Structure of constrained command filter.

In the design of the controller, we need the derivative of the virtual controller, so a large number of differential processes will affect the stability of the controller. Thus, command-filter is proposed to solve the problems of differential expansion and input saturation, besides that, it can also eliminate the time derivative of (24). The structure diagram of the command-filter is shown in Fig. 7. The state equation of command-filter can be described as

$$\begin{bmatrix} \dot{q}_1 \\ \dot{q}_2 \end{bmatrix} = \begin{bmatrix} q_2 \\ 2\xi\omega_n \left[S_R \left(\frac{\omega_n^2}{2\xi\omega_n} \right) (S_M(u) - q_1) - q_2 \right] \end{bmatrix} \tag{25}$$

where

$$\begin{bmatrix} q_1 \\ q_2 \end{bmatrix} = \begin{bmatrix} x^c \\ \dot{x}^c \end{bmatrix}, u = x^d \tag{26}$$

where ξ and ω_n are the damping and bandwidth of the filter, respectively. And $S_R(.)$ and $S_M(.)$ represent the rate and magnitude limit, respectively [24].

A filter error will be produced in the command-filter. We must redefine tracking error $\bar{e_1} = e_1 - \varepsilon_1$, and designed compensation signal is given by

$$\dot{\varepsilon}_1 = -k_1\varepsilon_1 + \frac{3E_d\hat{\eta}_1}{2u_{dc}}\left(i_d^c - \hat{i}_d^d\right) \tag{27}$$

In order to facilitate the subsequent calculation, according to (24) and (27), the $\dot{\bar{e}_1}$ can be calculated as

$$\begin{aligned}
\dot{\bar{e}_1} =& \frac{3E_d i_d \eta_1}{2u_{dc}} - \eta_1 i_{dc} - \dot{u}_{dc}^c + k_1\varepsilon_1 - \frac{3E_d\hat{\eta}_1}{2u_{dc}} i_d^c + \frac{3E_d\hat{\eta}_1}{2u_{dc}}\hat{i}_d^d \\
=& \frac{3E_d i_d\hat{\eta}_1}{2u_{dc}} + \frac{3E_d i_d\tilde{\eta}_1}{2u_{dc}} - \eta_1 i_{dc} - \dot{u}_{dc}^c + k_1\varepsilon_1 - \frac{3E_d\hat{\eta}_1}{2u_{dc}} i_d^c + \hat{\eta}_1 i_{dc} + \dot{u}_{dc}^c - k_1 e_1 \\
=& \frac{3E_d\hat{\eta}_1}{2u_{dc}} e_2 - k_1\bar{e}_1 + \tilde{\eta}_1\left(\frac{3E_d i_d}{2u_{dc}} - i_{dc}\right)
\end{aligned} \tag{28}$$

In the d-axis controller, we use the ordinary first order sliding mode defined as

$$S_1 = e_2 \tag{29}$$

We design the integral sliding mode for q-axis controller, and the q-axis integral sliding surface can be chosen as follows

$$S_2 = e_3 + \partial_1\int_0^t e_3 dt \tag{30}$$

Among them, $\partial_1 > 0$ represents a designed parameter. Then, the control objective is equivalent to the sliding surface $S_i = 0, i = 1, 2$.

At present, the following part is adaptive update law, the following Lyapunov function is selected to obtain the adaptive updated laws, and the dynamic stability of the response errors is obtained as following

$$V_2 = \frac{1}{2}\left(\bar{e_1}^2 + {S_1}^2 + {S_2}^2 + \frac{\tilde{\eta}_1^2}{\lambda_1} + \frac{\tilde{\eta}_2^2}{\lambda_2} + \frac{\tilde{\eta}_3^2}{\lambda_3}\right) \tag{31}$$

where λ_1, λ_2, and λ_3 denote the adaptive gains. $\tilde{\eta}_2 = \eta_2 - \hat{\eta}_2$ and $\tilde{\eta}_3 = \eta_3 - \hat{\eta}_3$ are the estimated errors of unknown parameters. The derivative of V_2 can be calculated as following

$$\dot{V}_2 = \bar{e}_1\dot{\bar{e}}_1 + S_1\dot{S}_1 + S_2\dot{S}_2 - \frac{\tilde{\eta}_1}{\lambda_1}\dot{\hat{\eta}}_1 - \frac{\tilde{\eta}_2}{\lambda_2}\dot{\hat{\eta}}_2 - \frac{\tilde{\eta}_3}{\lambda_3}\dot{\hat{\eta}}_3 \tag{32}$$

From equation (17), (18) and (22), we can get the derivative of sliding surfaces S_i, $i = 1, 2$ as

$$\begin{aligned}
\dot{S}_1 =& \dot{e}_2 \\
=& -\eta_2 i_d + \omega i_q + \eta_3(u_d - E_d) - \dot{i}_d^c \\
=& -\hat{\eta}_2 i_d - \tilde{\eta}_2 i_d + \omega i_q + \hat{\eta}_3(u_d - E_d) + \tilde{\eta}_3(u_d - E_d) - \dot{i}_d^c
\end{aligned} \tag{33}$$

$$\begin{aligned}
\dot{S}_2 =& \dot{e}_3 + \partial_1 e_3 \\
=& -\eta_2 i_q - \omega i_d + \eta_3\left(u_q - E_q\right) - \dot{i}_q^c + \partial_1 e_3 \\
=& -\hat{\eta}_2 i_q - \tilde{\eta}_2 i_q - \omega i_d + \hat{\eta}_3\left(u_q - E_q\right) + \tilde{\eta}_3\left(u_q - E_q\right) - \dot{i}_q^c + \partial_1 e_3
\end{aligned} \tag{34}$$

Taking equation (28), (33), (34) into equation (32), we then obtain

$$\begin{aligned}\dot{V}_2 = & S_1\left(\frac{3E_d\hat{\eta}_1}{2u_{dc}}\bar{e}_1 - \hat{\eta}_2 i_d + \omega i_q + \hat{\eta}_3\left(u_d - E_d\right) - \dot{i}_d^c\right) - k_1\vec{e}_1^2 \\ & + S_2\left(-\hat{\eta}_2 i_q - \omega i_d + \hat{\eta}_3\left(u_q - E_q\right) - \dot{i}_q^c + \partial_1 e_3\right) \\ & - \frac{\tilde{\eta}_1}{\lambda_1}\left(\dot{\hat{\eta}}_1 - \lambda_1\bar{e}_1\left(\frac{3E_d i_d}{2u_{dc}} - i_{dc}\right)\right) - \frac{\tilde{\eta}_2}{\lambda_2}\left(\dot{\hat{\eta}}_2 + \lambda_2 S_1 i_d + \lambda_2 S_2 i_q\right) \\ & - \frac{\tilde{\eta}_3}{\lambda_3}\left(\dot{\hat{\eta}}_3 - \lambda_3 S_1\left(u_d - E_d\right) - \lambda_3 S_2\left(u_q - E_q\right)\right)\end{aligned} \tag{35}$$

In order to eliminate this influence of η_1, η_2 and η_3, we design the projection-operator-based parameters adaptive law as follows

$$\begin{aligned}\dot{\hat{\eta}}_1 &= \lambda_1 \mathrm{Proj}\left(\hat{\eta}_1,\ \bar{e}_1\left(\frac{3E_d i_d}{2u_{dc}} - i_{dc}\right)\right) \\ \dot{\hat{\eta}}_2 &= \lambda_1 \mathrm{Proj}\left(\hat{\eta}_2,\ -\left(S_2 i_d + S_3 i_q\right)\right) \\ \dot{\hat{\eta}}_3 &= \lambda_3 \mathrm{Proj}\left(\hat{\eta}_3,\ S_2\left(u_d - E_d\right) + S_3\left(u_q - E_q\right)\right)\end{aligned} \tag{36}$$

where Proj $(\cdot,\cdot)$ denotes the projection operator [33-34]. The projection operator is valid for robust adaptive controller which needs multiple differentiation of the adaptive law. According to the projection operator, we have

$$\begin{aligned}&\tilde{\eta}_1\left[\bar{e}_1\left(\frac{3E_d i_d}{2u_{dc}} - i_{dc}\right) - \mathrm{Proj}\left(\hat{\eta}_1,\ \bar{e}_1\left(\frac{3E_d i_d}{2u_{dc}} - i_{dc}\right)\right)\right] \le 0 \\ &\tilde{\eta}_2\left[-S_2 i_d - S_3 i_q - \mathrm{Proj}\left(\hat{\eta}_2,\ -\left(S_2 i_d + S_3 i_q\right)\right)\right] \le 0 \\ &\tilde{\eta}_3\left[S_2\left(u_d - E_d\right) + S_3\left(u_q - E_q\right) - \mathrm{Proj}\left(\hat{\eta}_3,\ S_2\left(u_d - E_d\right) + S_3\left(u_q - E_q\right)\right)\right] \le 0\end{aligned} \tag{37}$$

Therefore, in view of above parameters adaptive update laws, equation (35) also is simplified as

$$\begin{aligned}\dot{V}_2 \le & S_1\left(\frac{3E_d\hat{\eta}_1}{2u_{dc}}\bar{e}_1 - \hat{\eta}_2 i_d + \omega i_q + \hat{\eta}_3\left(u_d - E_d\right) - \dot{i}_d^c\right) \\ & + S_2\left[-\hat{\eta}_2 i_q - \omega i_d + \hat{\eta}_3\left(u_q - E_q\right) - \dot{i}_q^c + \partial_1 e_3\right] - k_1\vec{e}_1^2\end{aligned} \tag{38}$$

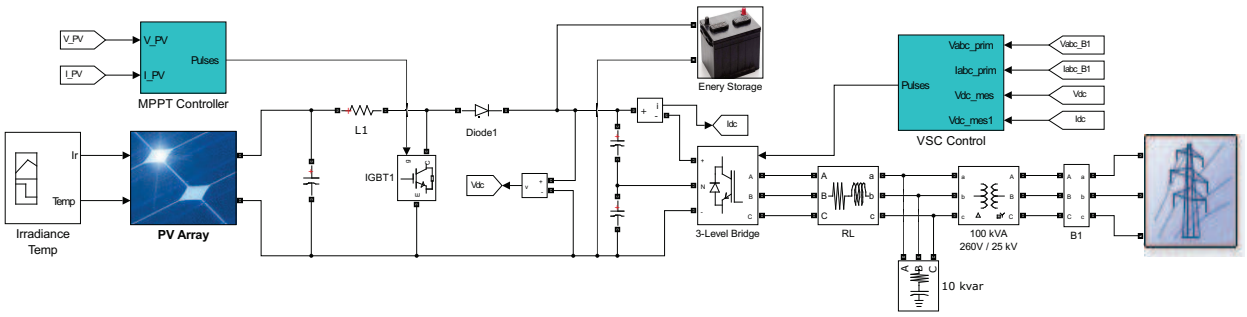

Figure 8: The simulation of BESS-PV grid-connected system.

In order to ensure the globally asymptotic stability of the whole PV grid-connected inverter. And the adaptive parameter estimated method and integral sliding mode control algorithm as a whole must ensure that $\dot{V}_2$ is negative semi-definite, namely, $\dot{V}_2 \le 0$, so that, we choose

$$\begin{aligned}-k_2\mathrm{sat}(S_1) &= -\frac{1}{\hat{\eta}_3}\left(\frac{3E_d\hat{\eta}_1}{2u_{dc}}\bar{e}_1 - \hat{\eta}_2 i_d + \omega i_q - \hat{\eta}_3 E_d - \dot{i}_d^c\right) \\ -k_3\mathrm{sat}(S_2) &= -\frac{1}{\hat{\eta}_3}\left(-\hat{\eta}_2 i_q - \omega i_d - \hat{\eta}_3 E_q - \dot{i}_q^c + \partial_1 e_3\right)\end{aligned} \tag{39}$$

Table 2: The Basic Parameters of BESS-PV Grid-Connected System

Parameters	Value
DC-link parameters	$C = 6$ (mF), $C_1 = 100$ (μF), $C_2 = 1$ (mF), $u_{dc}^c = 500$ (V)
	$L_1 = 5$ (mH), $L_2 = 1$ (mH)
AC-link parameters	$R = 2$ (mΩ), $L = 0.25$ (mH), $V_g = 260$ (V)
	f =60 (Hz), k_d=k_q = 10 kHz, T : 260 V / 25 kV
Controller parameters	$k_1 = 560$, $k_2 = 1500$, $k_3 = 50$, $\partial_1 = 2$
	$\eta_1 = 1000$, $\eta_2 = 2000$, $\eta_2 = 300$

where $k_2 > 0$, and $k_3 > 0$ represent the adjustable parameters, and the function sat($\cdot$) represents the saturation function defined as [35]

$$\text{sat}(S) = \begin{cases} 1, & S > \varphi \\ S/\varphi, & |S| \le \varphi \\ -1, & S < -\varphi \end{cases} \tag{40}$$

where, φ represents the sliding layer, which is defined between 0 and 0.5. Then the control law u_d and u_q can be acquired as

$$\begin{aligned} u_d &= -\frac{1}{\hat{\eta}_3}\left(\frac{3E_d\hat{\eta}_1}{2u_{dc}}\bar{e}_1 - \hat{\eta}_2 i_d + \omega i_q - \hat{\eta}_3 E_d - \dot{i}_d^c + k_2\text{sat}(S_1)\right) \\ u_q &= -\frac{1}{\hat{\eta}_3}\left(-\hat{\eta}_2 i_q - \omega i_d - \hat{\eta}_3 E_q - \dot{i}_q^c + \partial_1 e_3 + k_3\text{sat}(S_2)\right) \end{aligned} \tag{41}$$

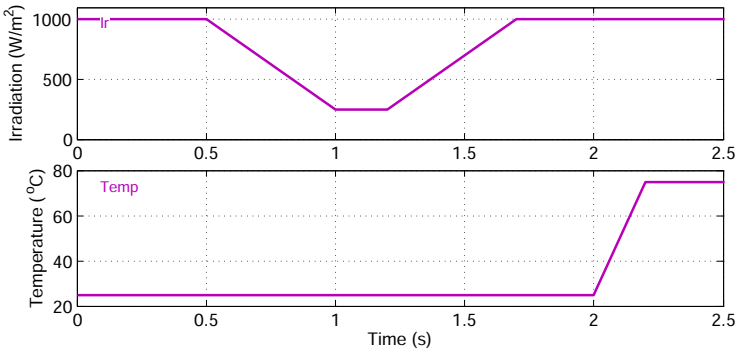

Figure 9: Solar irradiation and temperature change.

According to the above controller law, adaptive parameters estimation law and Barbalat's Lemma [36], the function is obtained as

$$\dot{V}_2 \le -k_1\bar{e}_1^2 - k_2 S_1\text{sat}(S_1) - k_3 S_2\text{sat}(S_2) \le 0 \tag{42}$$

From (42) we can see, the whole system will be asymptotically by using designed controller. The controller workflow is shown in Fig. 6.

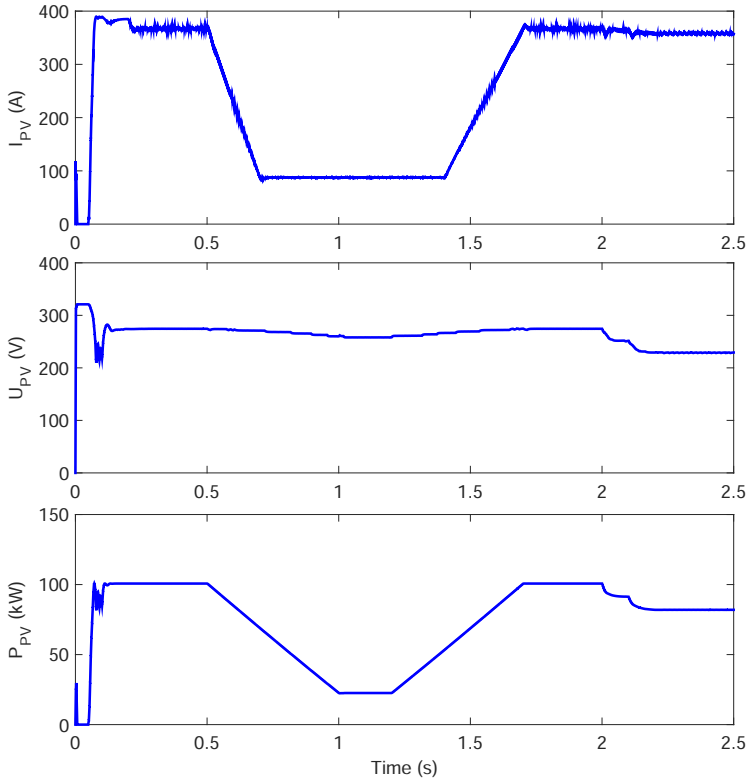

Figure 10: The output current, voltage and power of PV array.

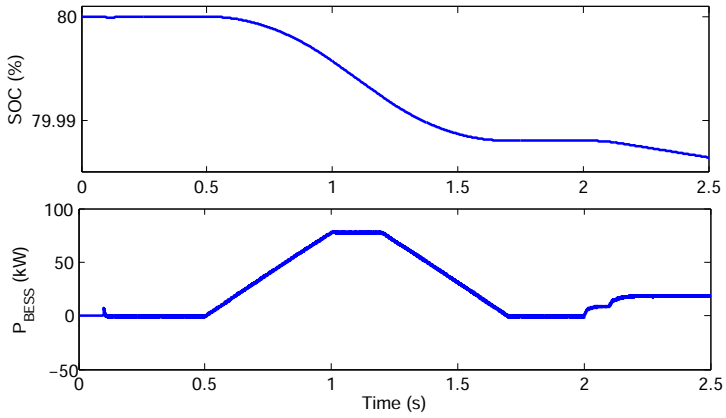

Figure 11: The battery's SOC and the power responses of the BESS.

4. Simulation Results

In order to verify the validity of the designed controller, we built a simulation model in MATLAB/simulink environment. And we primarily analyse the performance of dynamic, static, anti-jamming and robustness under the proposed control and PI control algorithms. The simulation model for the whole system is shown in Fig. 8, which is used to checkout the performance of the proposed controller. Moreover, the basic DC-link and AC-link parameters of system are list in Table 2.

The selection of controller parameters and adaptive parameters is very important for the control performance of

the designated position tracking, and the selection steps of controller parameters are as follows: 1) Firstly, the adaptive parameters λ_1, λ_2 and λ_3 are set to zero, which are used to substitute the accurate parameter estimation values. Then, we can try to adjust the parameters k_1, k_2 and k_3 according to Lyapunov stability theory to realize the command filter backstepping controller tracking for the PV grid-connected inverter. 2) As the larger adaptive parameters are set, the adaptive values are converged to the real value faster, but the larger the adaptive parameters will produce a larger overshoot, thus it is very important to adjust the controller parameter k_1, k_2 and k_3, and then adjust the adaptive parameters from small to large to obtain the appropriate adaptive parameters.

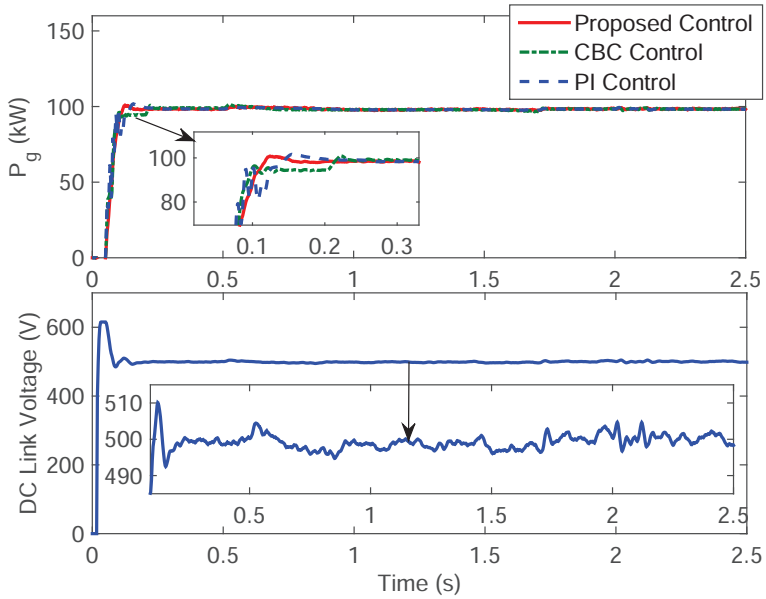

Figure 12: Active power and DC-link voltage.

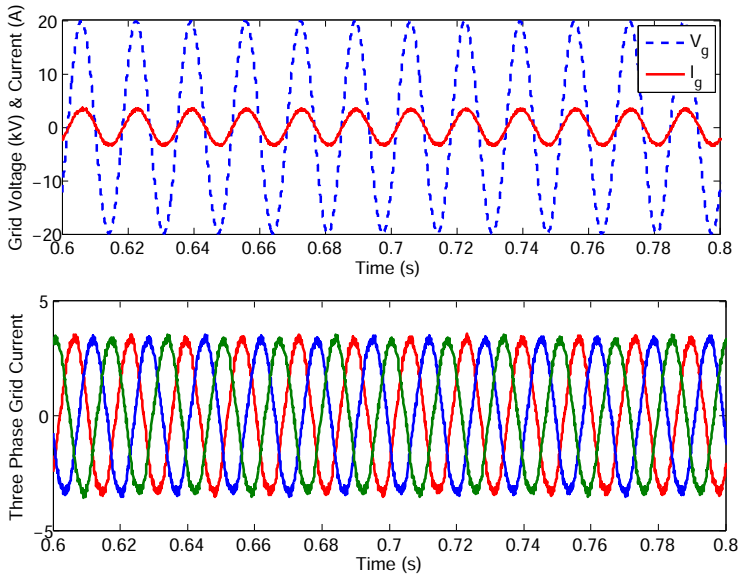

Figure 13: Grid voltage and current.

In order to obtain better control effect, according to the above steps, the specific simulation parameters and adaptive parameters can be seen in Table 2.

In this paper, the controller's capability is tested under the given solar irradiation and temperature change. From Fig. 9, we can see that the irradiation of the PV array is 1000 W/m^2 until $t = 0.5$s. Then the light radiation dropped to 250 W/m^2. After 0.2 s, the irradiation is rising to 1000 W/m^2. At same time, the ambient temperature of the first two seconds is maintained at 25 ^{o}C, and then the ambient temperature rises from 25 ^{o}C to 75 ^{o}C.

Fig. 10 shows the output current, voltage and power waveforms of the PV array. We can get from the diagram that the power is provided by the PV array varies with the intensity of light and the temperature of the environment.

Because of the fluctuation of the power generated by the PV array, so battery-energy-storage module is added to the DC side to compensate for the fluctuation. Fig. 11 shows the state of charge (SOC) of the battery and the compensation power is produced by battery-energy-storage.

Therefore, the out power from PV system to the grid is expressed in Fig. 12. From the Fig. 12, we can see that the designed controller in this paper has better performance, static following and stronger robustness than the command-filtered backstepping controller (CBC) and PI controller. Fig. 12 also shows that the DC voltage u_{dc} has a good following effect at the enactment value $u_{dc}^c = 500$ V. And the single-phase grid current with the grid voltage and the three-phase grid current is presented in Fig. 13.

When the system is working under changes in solar radiation, the quality of the output power of PV system will decline and can be described by THD, as shown in Fig. 14. It can be seen that the THD of the grid current injected by using the design controller is 1.88%, while the THD injected into the grid current is 2.06% of the CBC and 2.22% under PI controller.

From the above analysis of simulation results, the controller designed in this paper has better dynamic performance. Under various atmospheric and operating conditions, the proposed control method can make both the active power and the reactive power of the power grid better improve the power quality of the system output by comparing with the CBC and PI controller.

Fig. 15 shows the estimation of the system parameters by designed controller. From Fig. 15, the projection adaptive updated algorithm can online continuously approximate to the true value, and it can be in constant approximation adaptive law to effectively deal with the uncertain parameters of the PV system. Hence, the proposed controller has important application value for the PV system when the model parameters are unable to be obtained accurately. In order to observe the convergence of the adaptive curve, we give the adaptive curve of $t = 0 - 5s$. Fig. 16 depicts the sliding surface S_1 and integral sliding surface S_2. From Fig. 16, we observe that the designed controller can guarantee the robust convergence to the sliding surfaces $S_i = 0$, $i = 1, 2$.

5. Conclusion

In this paper, a projection adaptive command filtered backstepping controller is designed to deal with the issues of uncertainty of system parameters, the power fluctuation and the input saturation in the practical application of BESS-PV system. Meanwhile, the designed controller adaptively estimates the parameters of the system. Furthermore, the projection operator guarantees the bounded of the estimated parameters. And integral sliding mode is presented in the control system to enhance the robustness of the uncertainty. The simulation results show the comparison with the existing controller; the controller is designed to maintain steady operation under various operating conditions; the robustness, uncertainty of parameters and time-varying external disturbances are considered to provide a satisfactory performance. As can be seen from Fig. 12, the amplitude of the maximum fluctuation about the DC voltage does not exceed 2% of the reference voltage. Referring to Fig. 16, it can be seen that the sliding surface S_1 is controlled to be about plus or minus 0.2, and the sliding surface S_2 is controlled between -0.4 and 0.2.

Acknowledgment

This work was partially supported by the National Natural Science Foundation of China (61503156), National Key Research and Development Program (2016YFD0400301), Open Research Fund of Jiangsu Collaborative Innovation Center for Smart Distribution Network, Nanjing Institute of Technology (XTCX201806), National first-class discipline program of Food Science and Technology (JUFSTR20180205), and State Grid Zhejiang Province Technology Project (SGTYHT/17-JS-201).

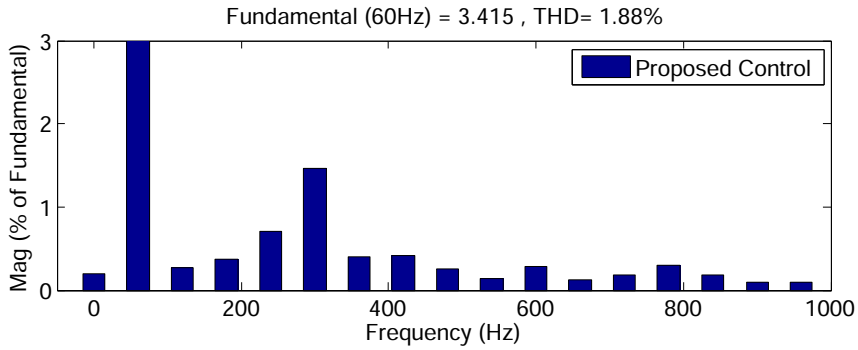

(a) THD in the proposed controller.

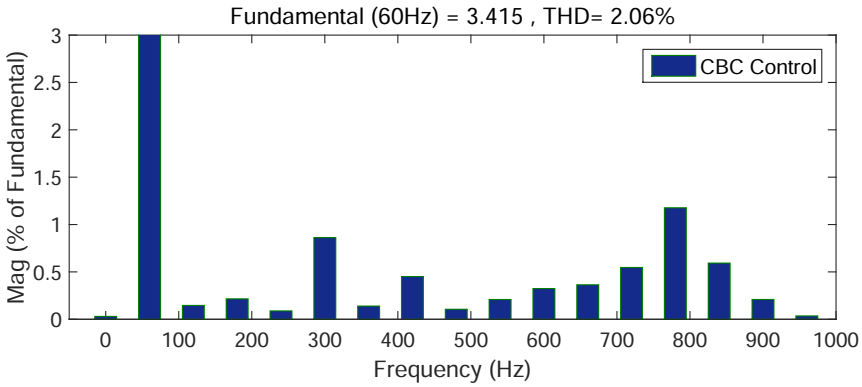

(b) THD in the CBC controller.

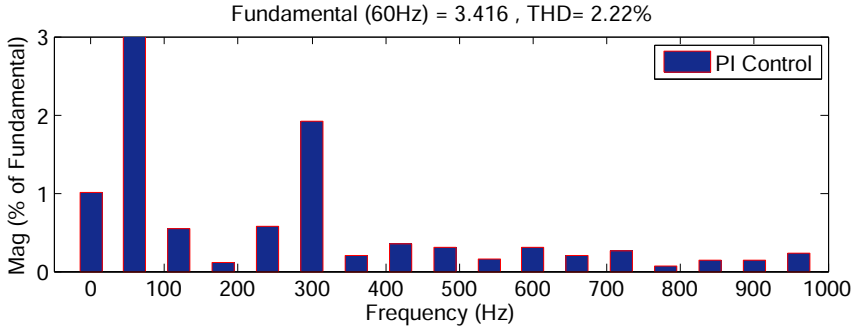

(c) THD in the PI controller.

Figure 14: THD in grid current with the change of irradiation and temperature.

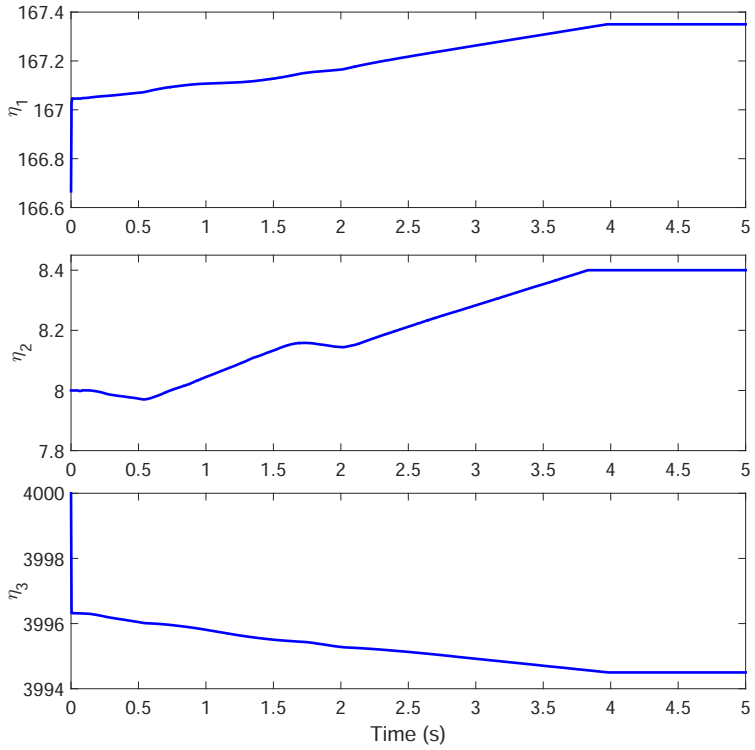

Figure 15: Adaptive unknown parameter responses for η_1, η_2 and η_3.

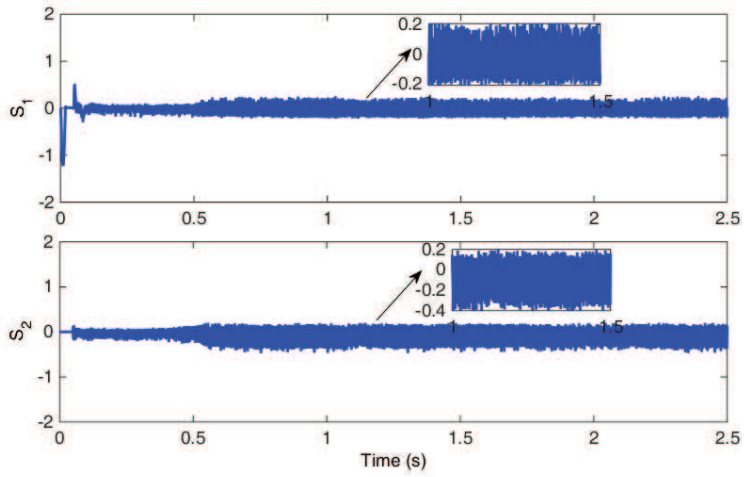

Figure 16: The responses of sliding mode surfaces S_1 and S_2.

References

[1] R. Teodorescu, M. Liserre, P. Rodrłguez, “Grid converters for photovoltaic and wind power systems”, Wiley, New York, 2011.
[2] J. M. Carrasco, L. G. Franquelo, J. T. Bialasiewicz, et al, “Power-electronic systems for the grid integration of renewable energy sources: a survey”, *IEEE Transactions on Industrial Electronics*, 53(2006), pp. 1002-1016.
[3] G. Dileep, S. N. Singh, “Application of soft computing techniques for maximum power point tracking of SPV system”, *Solar Energy*, 141(2017), pp. 182-202,.

[4] B. N. Alajmi, K. H. Ahmed, S. J. Finney, et al, "Fuzzy-logic control approach of a modified hill-climbing method for maximum power point in microgrid standalone PV system", *IEEE Transaction on Power Electronics*, 26(2011), pp. 1022-1030.

[5] J. Liu, W. Luo, X. Yang, et al, "Robust model-based fault diagnosis for PEM fuel cell air-feed system", *IEEE Transactions on Industrial Electronics*, 63(2016), pp. 3261-3270.

[6] Y. Yang, Q. Ye, L. Tung, et al, "Integrated size and energy management design of battery storage to enhance grid integration of large-scale PV power plants", *IEEE Transactions on Industrial Electronics*, 65(2018), pp. 394-402.

[7] A. Kouchaki, H. Iman-Eini, B. Asaei, "A new maximum power point tracking strategy for PV arrays under uniform and non-uniform insolation conditions", *Solar Energy*, 91(2013), pp. 221-232.

[8] M. H. Moradi, A. R. Reisi, "A hybrid maximum power point tracking method for photovoltaic systems", *Solar Energy*, 85(2011), pp. 2965-2976.

[9] M. B. Delghavi, S. Shoja-Majidabad and A. Yazdani, "Fractional-order sliding-mode control of islanded distributed energy resource systems", *IEEE Transactions on Sustainable Energy*, 7(2016), pp. 1482-1491.

[10] M. B. Delghavi and A. Yazdani, "Islanded-mode control of electronically coupled distributed-resource units under unbalanced and nonlinear load conditions", *IEEE Transactions on Power Delivery*, 26(2011), pp. 661-673.

[11] S. Ouchen, S. Abdeddaim, A. Betka, A. Menadi, "Experimental validation of sliding mode-predictive direct power control of a grid connected photovoltaic system, feeding a nonlinear load", *Solar Energy*, 137(2016), pp. 328-336.

[12] J. I. Leon, S. Vazquez, L. G. Franquelo, "Multilevel converters: control and modulation techniques for their operation and industrial applications", *Proceedings of the IEEE*, 105(2017), pp. 2066-2081.

[13] F. D. Franco, T. V. Vu, D. Gonsulin, H. Vahedi, C. S. Edrington, "Enhanced performance of PV power control using model predictive control", *Solar Energy*, 158(2017), pp. 679-686.

[14] R. Bakhshi, J. Sadeh, "Voltage positive feedback based active method for islanding detection of photovoltaic system with string inverter using sliding mode controller", *Solar Energy*, 137(2016), pp. 564-577.

[15] K. A. Hosani, A. Malinin, V. I. Utkin, "Sliding mode PID control of buck converters", *2009 European Control Conference (ECC)*, Budapest, Hungary, 15034467, 23-26 Aug. 2009.

[16] B. Yang, T. Yu, H. Shu, D. Zhu, N. An, Y. Sang, L. Jiang, "Energy reshaping based passive fractional-order PID control design and implementation of a grid-connected PV inverter for MPPT using grouped grey wolf optimizer", *Solar Energy*, 170(2018), pp. 31-46.

[17] T. K. Roy, M. A. Mahmud, "Active power control of three-phase grid-connected solar PV systems using a robust nonlinear adaptive backstepping approach", *Solar Energy*, 153(2017), pp. 64-76.

[18] J. A. Cortajarena, O. Barambones, P. Alkorta, J. D. Marcos, "Extended state observer based sliding mode control for three-phase power converters". *Solar Energy*, 155(2017), pp. 793-804.

[19] K. N. E. K. Ahmad, N. A. Rahim, J. Selvaraj, A. Rivai, K. Chaniago, "An effective passive islanding detection method for PV single-phase grid-connected inverter", *Solar Energy*, 97(2013), pp. 155-167.

[20] A. D. Martin, J. M. Cano, J. F. A. Silva, et al, "Backstepping control of smart grid-connected distributed photovoltaic power supplies for telecom equipment", *IEEE Transactions on Energy Conversion*, 30(2015), pp. 1496-1504.

[21] M. R. Mojallizadeh, M. A. Badamchizadeh, "Second-order fuzzy sliding-mode control of photovoltaic power generation systems", *Solar Energy*, 149(2017), pp. 332-340.

[22] R. Wai, C. Lin, W. Wu, H. Huang, "Design of backstepping control for high-performance inverter with stand-alone and grid-connected power-supply modes", *IET Power Electronics*, 6(2013), pp. 752-762.

[23] S. Dhar, and P. K. Dash, "A new backstepping finite time sliding mode control of grid connected PV system using multivariable dynamic VSC model", *International Journal of Electrical Power & Energy Systems*, 82(2016), pp. 314-330.

[24] B. Jiang, D.Xu, P. Shi, "Adaptive neural observer-based backstepping fault tolerant control for near space vehicle under control effector damage", *IET Control Theory and Applications*, 8(2014), pp. 658-666.

[25] C. S. Ting, Y. N. Chang, B. W. Shi and J. F. Lieu, "Adaptive backstepping control for permanent magnet linear synchronous motor servo drive", *IET Electric Power Applications*, 9(2015), pp. 265-279.

[26] J. Yu, P. Shi, W. Dong, et al, "Neural network based adaptive dynamic surface control for permanent magnet synchronous motors", *IEEE Transactions on Neural Networks and Learning Systems*, 26(2015), pp. 640-645.

[27] J. Yu, P. Shi, W. Dong, et al, "Observer and command-flter-based adaptive fuzzy output feedback control of uncertain nonlinear systems", *IEEE Transactions on Industrial Electronics*, 62(2015), pp. 5962-5970.

[28] W. Dong, J. A. Farrell, M. M. Polycarpou, et al, "Command filtered adaptive backstepping", *IEEE Transactions on Control Systems Technology*, 20(2012), pp. 566-580.

[29] J. A. Farrell, M. Polycarpou, M. Sharma, et al, "Command filtered backstepping", *IEEE Transactions on Automatic Control*, 54(2009), pp. 1391-1395.

[30] F. Belhachat, C. Larbes, "Modeling, analysis and comparison of solar photovoltaic array configurations under partial shading conditions", *Solar Energy*, 120(2015), pp. 399-418.

[31] R. Ahmad, A. F. Murtaza, U. T. Shami, Zulqarnain, F. Spertino, "An MPPT technique for unshaded/shaded photovoltaic array based on transient evolution of series capacitor", *Solar Energy*, 157(2017), pp. 377-389.

[32] V. Utkin, "Variable structure systems with sliding modes", *IEEE Transactions on Automatic Control*, 22(2003), pp. 212-222.

[33] H. Chen, H. Wang, "Numerical simulation for conservative fractional diffusion equations by an expanded mixed formulation", *Journal of Computational & Applied Mathematics*, 296(2016), pp. 480-498.

[34] V. Aggarwal, A. R. Calderbank, "Boolean functions, projection operators, and quantum error correcting codes", *IEEE Transactions on Information Theory*, 54(2008), pp. 1700-1707.

[35] N. Kumar, T. K. Saha, J. Dey, "Sliding mode control, implementation and performance analysis of standalone PV fed dual inverter," *Solar Energy*, 155(2017), pp. 1178-1187.

[36] H. A. Najafabadi, N. Ozalp, "Aperture size adjustment using model based adaptive control strategy to regulate temperature in a solar receiver", *Solar Energy*, 159(2018), pp. 20-36.